

# Regularized Training of Intermediate Layers for Generative Models for Inverse Problems

Sean Gunn<sup>1</sup>, Jorio Cocola<sup>2</sup>, and Paul Hand<sup>1,2</sup>

<sup>1</sup>Khoury College of Computer Sciences, Northeastern University

<sup>2</sup>Department of Mathematics, Northeastern University

## Abstract

Generative Adversarial Networks (GANs) have been shown to be powerful and flexible priors when solving inverse problems. One challenge of using them is overcoming representation error, the fundamental limitation of the network in representing any particular signal. Recently, multiple proposed inversion algorithms reduce representation error by optimizing over intermediate layer representations. These methods are typically applied to generative models that were trained agnostic of the downstream inversion algorithm. In our work, we introduce a principle that if a generative model is intended for inversion using an algorithm based on optimization of intermediate layers, it should be trained in a way that regularizes those intermediate layers. We instantiate this principle for two notable recent inversion algorithms: Intermediate Layer Optimization and the Multi-Code GAN prior. For both of these inversion algorithms, we introduce a new regularized GAN training algorithm and demonstrate that the learned generative model results in lower reconstruction errors across a wide range of under sampling ratios when solving compressed sensing, inpainting, and super-resolution problems.

## 1 Introduction

The task in an inverse problem is to estimate an unknown signal given a (possibly noisy) set of measurements of that signal. In practice, inverse problems are often ill-posed, which often require the incorporation of prior information about the target signal to recover a reasonable estimate of it.

Deep generative models have demonstrated remarkable performance when used as priors for solving inverse problems [6, 4, 12, 24, 23, 25, 26]. Typically, a

generative modeling-based approach for inverse problems has two phases: a training phase and an inversion/deployment phase. In the first phase, a generative network is trained on a dataset of images different from the data in the testing phase. After training, the network parameters are typically fixed and an optimization problem involving the known forward model is solved to estimate an unknown signal of interest. An advantage of this class of methods is that the prior can be trained entirely in an unsupervised manner and without previous knowledge of the specific inverse problem that needs to be solved downstream. This allows the trained network to be used for a variety of inverse problems.

Some generative networks explicitly map a low-dimensional input to a high-dimensional signal space. The outputs of the generative network therefore have a low intrinsic dimensionality. While this is useful for regularizing the inverse problem, it can limit the expressivity of the network and lead to *representation error*, the error between the target signal and the closest signal in the range of the generative network.

Several recent methods have attempted to reduce representation error by introducing optimization algorithms that enlarge the search space of the inversion algorithm. These include methods that optimize both over the input of the network as well as over the activations of one or more intermediate layers. Examples of this class of inversion methods include Intermediate Layer Optimization (ILO) [7], GAN Surgery [29], and the Multi-code GAN Prior (mGANprior) [10]. These algorithms were applied to state-of-the-art off-the-shelf GANs, such as PGGAN and StyleGAN [17, 19], which were trained agnostic to the specific optimization algorithm that would be used for inversion. Consequently, the inversion algorithms optimize over a regions of the space of intermediate presentations that were not regularized during training. This suggests that it may be possible to improve the reconstruction performance of these algorithms by explicitly regu-

---

Sean Gunn <gunn.s@northeastern.edu>  
 Jorio Cocola <cocola.j@northeastern.edu>  
 Paul Hand <p.hand@northeastern.edu>  
 Github Link : <https://github.com/g33sean/RTIL>

larizing the intermediate layers during the training phase. In this paper we confirm this hypothesis.

We consider the problem of training a GAN that will be used for solving inverse problems via an inversion algorithm that optimizes over intermediate layers. We put forward the following principle termed *Regularized Training of Intermediate Layers (RTIL)*:

*If a GAN’s intermediate layers are optimized during inversion, they should be regularized during training.*

We use this principle to derive new training algorithms for GANs that are intended for solving inverse problems. For both ILO and the mGANprior, we introduce a new training algorithm for StyleGAN and PGGAN, respectively. For these new trained GANs, we achieve improved reconstruction quality relative to the corresponding GANs trained without the principle.

This principle may lead to the following workflow for solving inverse problems with GANs. First, train a generative network with latent variable  $z_0$ , sampled from a latent distribution  $p_{z_0}$ , and outputting signals  $x$  from the target distribution (Figure 1 Step 1). Second, explore various inversion algorithms, including some that optimize over intermediate layers by introducing an additional optimization variable  $z_1$  (Figure 1 Step 2). Algorithms of this type include ILO and mGANprior. Third, if such an algorithm provides competitive performance for inversion, then use RTIL to devise a new GAN training algorithm. This can be achieved by introducing a new latent variable  $z_1 \sim p_{z_1}$  where  $p_{z_1}$  is an appropriate probability distribution (Figure 1 Step 3). Finally, during deployment, use this trained generative network for inverse problems via the selected inversion algorithm (Figure 1 Step 4).

This workflow demonstrates a way to use recently introduced inversion algorithms in order to inspire new training algorithms for GANs. It provides additional ways of training GANs knowing that they will be used for inversion, and it provides a way to ensure that some empirically successful inversion algorithms are operating in a more principled manner by ensuring they are searching over a space of parameters that has been suitably regularized.

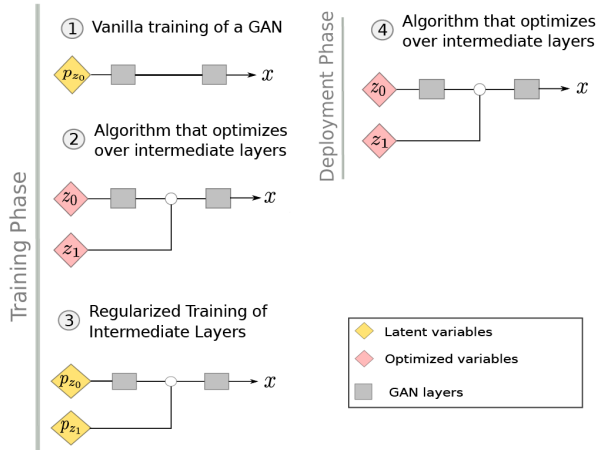


Figure 1: The workflow for using Regularized Training of Intermediate Layers (RTIL) to develop new training algorithms of GANs that will be used for inversion. See the text for details.

The contributions of this paper are the following.

- We introduce Regularized Training of Intermediate Layers, a principle for training deep generative networks that are intended to be used for inverse problems with an optimization algorithm that optimizes over intermediate layer representations.
- In the case of Intermediate Layer Optimization, we use our principle to devise a novel GAN training algorithm. With the resulting trained GAN, we demonstrate lower reconstruction errors (compared to GAN training without the principle) for compressed sensing, inpainting, and super resolution over a wide range of under sampling ratio.
- We show the versatility of the method by repeating the same contribution in the case of the Multi-Code GAN Prior.
- We illustrate the benefits of compressed sensing with RTIL by theoretically showing that a model trained without regularizing intermediate layers has a strictly larger reconstruction error than a model where the intermediate layers were regularized during training. For simplicity, this result is established in the case of a two layer linear neural network trained in a supervised setting.

## 1.1 Related Works

In the recent years, various approaches have been proposed for dealing with the representation error when solving inverse problems with a learned generative prior. As described above, there is one class of approaches that focus on enlarging the latent space dimension either at training or at inversion time [4, 8, 14]. On the other hand, there is another notable class of approaches recently put forward is based on flow-based invertible neural networks. These generative networks have invertible architectures and a latent space with the same size of the image space, and thus have zero representation error [1, 3, 22, 20, 28, 34, 33, 13]. Both these type of approaches attempt to limit the representation error during training or inversion.

Similarly to flow-based models, score networks and subsequent variants [30, 31, 32] have support on the entire signal space, allow for conditional sampling and likelihood estimation, and have been object of recent interests for their use in inverse problems [27, 16, 15].

The increased representation power of the above mentioned generative networks, comes usually at a price of increased computational cost both during the training and the inversion phase. In contrast, our proposed principle leads to training algorithms that have essentially the same computational cost as the standard ones, also leaving the cost of the inversion algorithms the same.

## 2 Generative Models and Optimization Algorithms for Inverse Problems

### 2.1 Background

We consider the problem of training a GAN for the use of a prior for solving inverse problems. We consider a GAN  $G$  which maps a latent space  $\mathbb{R}^{n_0}$  to an image space  $\mathbb{R}^{n_d}$ , where  $n_0 \ll n_d$ . In this paper, we focus on the linear imaging inverse problems of compressed sensing, inpainting, and superresolution, though our proposed method also applies to nonlinear inverse problems such as phase retrieval, and inversion problems about non-image signals. We consider the general linear inverse problem of recovering an image  $x \in \mathbb{R}^{n_d}$  from a set of linear measurements  $y \in \mathbb{R}^m$ , given by  $y = \mathcal{A}(x)$ , where  $\mathcal{A} : \mathbb{R}^{n_d} \rightarrow \mathbb{R}^m$  is a forward linear measurement operator. We study only the noiseless case, but our method easily extends to case with measurement noise. In this paper we study measurement operators  $\mathcal{A}$  of the following form:

- Compressed Sensing:  $\mathcal{A} = A \in \mathbb{R}^{m \times n_d}$ ,  $A$  is a random matrix that samples from a known distribution with  $m < n_d$ .
- Inpainting:  $\mathcal{A} = M \in \mathbb{R}^{m \times n_d}$ ,  $M$  is a masking matrix with binary entries.
- Super-Resolution:  $\mathcal{A} = S_{m_\downarrow} \in \mathbb{R}^{m \times n_d}$  where  $S_{m_\downarrow}$  is the downsampling operator with downsampling factor  $m_\downarrow$ .

An estimate of  $x$  can be recovered by finding the image in the range of  $G$  that is most consistent with the measurements  $y$  in the following sense, as introduced in [6]. First, solve

$$\hat{z}_0 = \arg \min_{z_0} \|y - \mathcal{A}(G(z_0))\|, \quad (1)$$

then, the estimate of  $x_0$  is given by  $G(z_0)$ .

As mentioned in the introduction, a difficulty of this optimization approach is that the estimated images are constrained to live within the range of  $G$ , which is a  $n_0$ -dimensional manifold in  $\mathbb{R}^{n_d}$ . Most images  $x_0$  will not live exactly in this range, and thus the method is limited by the representation error  $\min_{z_0} \|x_0 - G(z_0)\|$ .

In the next sections we review two recent algorithms for mitigating representation error during inversion. For ease of exposition, we will discuss the case where only one intermediate layer representation is optimized. We write  $G = g_1 \circ g_0$  where  $g_0 : \mathbb{R}^{n_0} \rightarrow \mathbb{R}^{n_1}$  and  $g_1 : \mathbb{R}^{n_1} \rightarrow \mathbb{R}^{n_d}$ .

### 2.2 Intermediate Layer Optimization (ILO) [7]

Given a trained generative model  $G = g_1 \circ g_0$ , Intermediate Layer Optimization (ILO) extends the range of the generative model by sequentially optimizing over each layer of the network, as demonstrated in Algorithm 1. The initial step begins exactly as in [6] by optimizing over the input vector  $z_0 \in \mathbb{R}^{n_0}$ . The solution is obtained in line 3, by initializing a  $z_0 \sim \mathcal{N}(0, I_{n_0})$ , then optimizing the loss with gradient descent. After the solution  $\hat{z}_0$  is obtained, the algorithm searches for a perturbation  $\hat{z}_1$  of  $g_0(\hat{z}_0)$  that further minimizes the reconstruction error (line 4). The final approximation of the target image  $x$  is given by  $g_1(\hat{z}_1 + g_0(\hat{z}_0))$ . As the authors point out, there are multiple ways where ILO can be regularized, including by an L1 penalty in the intermediate representation, or via early stopping. For the present paper, we present the method with early stopping as this was the method used by the publicly available code from the authors. Throughout this paper, we use the code provided by the authors when solving ILO.

**Algorithm 1** Intermediate Layer Optimization (ILO) for Compressed Sensing [7].

- 1: **Input:**  $G = g_1 \circ g_0$ , measurement matrix  $A \in \mathbb{R}^{m \times n_d}$ , compressed measurements  $y$ .
- 2: **Output:** estimated image  $\hat{x}$
- 3:  $\hat{z}_0 = \arg \min_{z_0} \|y - Ag_1(g_0(z_0))\|$  Initialize at  $z_0 \sim \mathcal{N}(0, I_{n_0})$
- 4:  $\hat{z}_1 = \arg \min_{z_1} \|y - Ag_1(z_1 + g_0(\hat{z}_0))\|$
- 5: Return:  $\hat{x} = g_1(\hat{z}_1 + g_0(\hat{z}_0))$

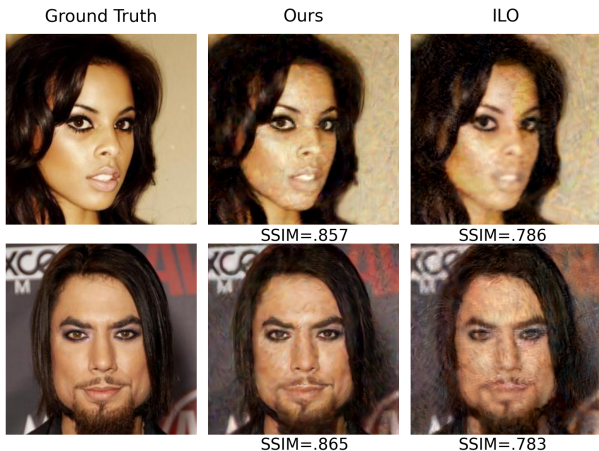


Figure 2: Comparison between ILO-RTIL (ours) and ILO for compressed sensing for 3% of measurements.

### 2.3 Multi-Code GAN (mGanPrior)

Multi-Code GAN Prior is an inversion method that simultaneously optimizes over multiple latent codes and composes their corresponding intermediate feature maps with adaptive channel importance. This effectively extends the expressivity of the network by giving it a higher dimensional input space and additional parameters to control the importance of each channels in the intermediate layer representation.

Assume we are given a pre-trained generative model  $G = g_1 \circ g_0$ , where the output of the first layer  $g_0$  has dimension  $H_1 \times W_1 \times C_1$  with  $C_1$  being the number of channels. Furthermore, chose  $N$  latent codes  $\{z_0^k\}_{k=1}^N \in \mathbb{R}^{n_0}$  and channel importance  $\{\alpha^k\}_{k=1}^N \in \mathbb{R}^{C_1}$ . Then the Multi-Code GAN Prior extended architecture computes  $g_1(\sum_{k=1}^N g_0(z_0^k) \odot \alpha^k)$  where  $\{g_0(z_0^k) \odot \alpha^k\}_{ijc} = \{g_0(z_0^k)\}_{ijc} \cdot \{\alpha^k\}_c$  is channel-wise multiplication,  $i, j$  are spatial location, and  $c$  is the channel index.

During the inversion phase the Multi-Code GAN Prior method optimizes over both the latent vectors  $\{z_0^k\}_{k=1}^N$  and the channel importance  $\{\alpha^k\}_{k=1}^N$  (Algorithm 2).

**Algorithm 2** Multi-Code GAN (mGANprior) [10].

- 1: **Input:** Trained network  $G = g_1 \circ g_0$ , latent codes  $\{z_0^k\}_{k=1}^N \in \mathbb{R}^{n_0}$ ,  $\{\alpha^k\}_{k=1}^N \in \mathbb{R}^{n_1}$ , measurement matrix  $A \in \mathbb{R}^{m \times n_d}$ , compressed measurements  $y$ .
- 2: **Output:** estimated image  $\hat{x}$
- 3: Initialize  $\{z_0^k\}_{k=1}^N \sim p_z, \{\alpha^k\}_{k=1}^N \sim p_\alpha$
- 4:  $\hat{z}, \hat{\alpha} = \arg \min_{\{z_0^k\}_{k=1}^N, \{\alpha^k\}_{k=1}^N} \|y - Ag_1(\sum_{k=1}^N g_0(z_0^k) \odot \alpha^k)\|$
- 5: Return:  $\hat{x} = g_1(\sum_{k=1}^N g_0(\hat{z}_0^k) \odot \hat{\alpha}^k)$



Figure 3: Comparison between mGANprior-RTIL (ours) and mGAN for compressed sensing for 5% of measurements.

### 3 RTIL

In this section, we present how the principle of Regularized Training of Intermediate Layers (RTIL) inspires training algorithms for GANs that are intended for inversion by Intermediate Layer Optimization (Section 3.1) and mGANprior (Section 3.2).

We consider the case of a practitioner having chosen, after some initial exploration, a base generative network  $G$  for use as prior in solving inverse problems. For simplicity in this section we will consider  $G = g_1 \circ g_0$  where  $g_0 : \mathbb{R}^{n_0} \rightarrow \mathbb{R}^{n_1}$  and  $g_1 : \mathbb{R}^{n_1} \rightarrow \mathbb{R}^{n_d}$ . The input latent vectors  $z_0$  of the network  $G_\theta^0$  are sampled from  $p_{z_0}$  (e.g.  $p_{z_0} = \mathcal{N}(0, I_{n_0})$ ) and  $\theta$  is the set of trained parameters.

We assume, furthermore, that the practitioner has selected an inversion algorithm that optimizes over the latent variable  $z_0$  and the intermediate layer between  $g_0$  and  $g_1$  of  $G$ . Optimizing over the intermediate layer corresponds to introducing a free variable  $z_1$  between  $g_0$  and  $g_1$  (Figure 4 left).

The RTIL principle states that if one intends to solve inverse problems by means of intermediate layer optimization algorithms, then *intermediate layers op-*



timized over during inversion should be regularized during training.

This principle can be used to design a new training algorithm in the following manner. We identify the additional free variable,  $z_1$ , used for optimization over the intermediate layer, consider it as a latent variable of the generative model, and provide it with a simple distribution  $p_{z_1}$ . For example, this could result in a generative model  $\tilde{G} : \mathbb{R}^{n_0 \times n_1} \rightarrow \mathbb{R}^{n_d}$ , such that  $\tilde{G}(z_0, z_1) = g_1(z_1 + g_0(z_0))$ , but could have alternative functional forms. This generative model reduces to the base generative model  $G : \mathbb{R}^{n_0} \mapsto \mathbb{R}^{n_d}$  if  $z_1$  is suitably chosen, for example if  $z_1 = 0$ .

The introduction of the latent variable  $z_1$  explicitly increases the dimensionality of the latent space. In practice, training latent variable models with high-dimensional latent spaces can be challenging and require careful regularization [4]. We address this difficulty by concurrently training the lower and higher dimensional models  $G_\theta$  and  $\tilde{G}_\theta$ , which share trainable weights  $\theta$  (Figure 4 right).

We train  $G_\theta$  and  $\tilde{G}_\theta$  via the following minimax formulation [9]

$$\begin{aligned} \min_{\theta} \max_{\Theta} \mathbb{E}_{x \sim p_x} [\log D_{\Theta}(x)] \\ + \frac{1}{2} \mathbb{E}_{\substack{z_0 \sim p_{z_0} \\ z_1 \sim p_{z_1}}} [\log(1 - D_{\Theta}(G_{\theta}(z_0)) \\ + \log(1 - D_{\Theta}(\tilde{G}_{\theta}(z_0, z_1))], \end{aligned}$$

where  $D_{\Theta} : \mathbb{R}^{n_d} \rightarrow \mathbb{R}$  is the discriminative network. This method could be extended to alternative GAN and non-GAN formulations [2, 11, 5].

Once  $\tilde{G}$  is trained, a practitioner could solve an inverse problem with forward operator  $\mathcal{A}$  by solving

$$\hat{z}_0, \hat{z}_1 = \arg \min_{z_0, z_1} \|y_0 - \mathcal{A}(\tilde{G}(z_0, z_1))\|,$$

using the selected optimization algorithm, resulting in  $\tilde{G}(\hat{z}_0, \hat{z}_1)$  as the estimate of the signal.

In this section, we considered the case where only one intermediate layer was optimized. The proposed method can directly extend to the case where multiple layers are optimized.

We will next describing the details of the application of RTIL in the case of Intermediate Layer Optimization and the Multi-Code GAN Prior.

### 3.1 RTIL for ILO

In the case of Intermediate Layer Optimization (ILO), we now present how to use RTIL to design a GAN training algorithm. Consider the base generative network  $G(z_0) = g_1(g_0(z_0))$ , to be used for inversion with

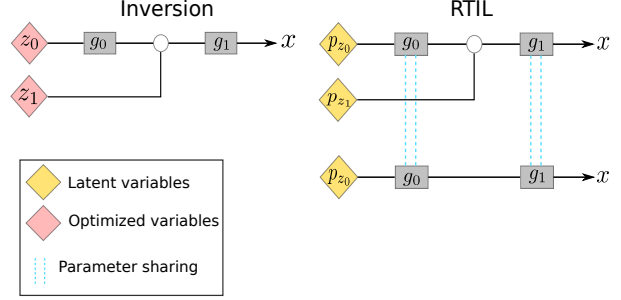


Figure 4: Visual representation of the RTIL principle. An inversion method that optimizes over intermediate layers informs the training of a family of generative networks adapted to that inversion method.

Intermediate Layer Optimization. ILO (Algorithm 1) extends the range of the network by optimizing  $g_1(z_1 + g_0(z_0))$  over latent variables  $z_0$  and  $z_1$ . Consequently, we consider the higher dimensional model generative model

$$\begin{aligned} \tilde{G}(z_0, z_1) &= g_1(z_1 + g_0(z_0)) \\ z_0 &\sim \mathcal{N}(0, I_{n_0}) \\ z_1 &\sim \mathcal{N}(0, \sigma^2 I_{n_1}), \end{aligned}$$

where  $\sigma^2$  is a hyperparameter. Then simultaneously the lower dimensional model  $G(z_0)$  and higher dimensional model  $\tilde{G}(z_0, z_1)$  are trained with the min max formulation above. Note  $z_0 \sim p_{z_0}$  and  $z_1 \sim p_{z_1}$  where Figure 5 depicts this process.

### 3.2 RTIL for mGANprior

In the case of Multi-Code GAN Prior method, we now present how to use RTIL to design a GAN training algorithm. Consider the base generative network  $G_\theta^0$  to be used for inversion with the Multi-Code GAN Prior method. The mGANprior Algorithm (Algorithm 2) extends the range of the network by optimizing  $g_1(\sum_{k=1}^N g_0(z_0^k) \odot \alpha^k)$  over latent variables  $z_0$  and  $z_1$ . Consequently, training the higher dimensional model yields

$$\begin{aligned} \tilde{G}(z_0^1, \dots, z_0^N, \alpha^1, \dots, \alpha^N) &= g_1\left(\sum_{k=1}^N g_0(z_0^k) \odot \alpha^k\right) \\ z_0^k &\sim \mathcal{N}(0, I_{n_0}) \\ p_{\alpha'} &\sim \text{Dir}_N(1) \end{aligned}$$

Specifically, a vector  $\alpha' \in \mathbb{R}^N$  is sampled from  $p_{\alpha'} \sim \text{Dir}_N(1)$ , where  $\text{Dir}_N(1)$  is the flat Dirichlet distribution, i.e. the uniform distribution over the  $(N - 1)$ -dimensional simplex. Then each vector  $\alpha^k$

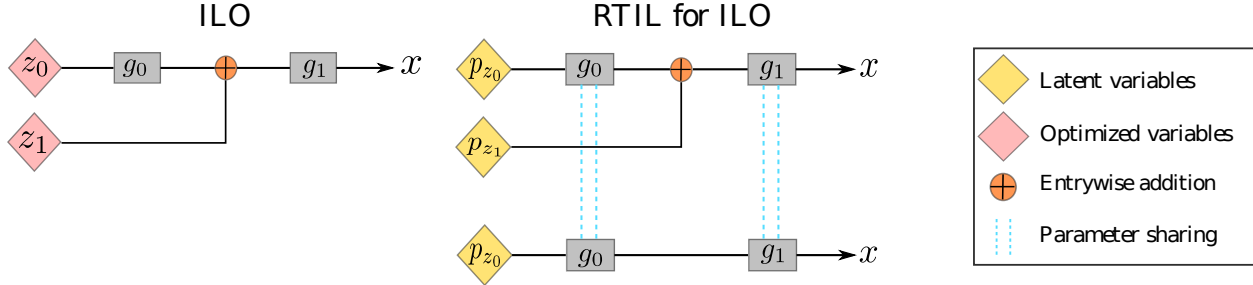


Figure 5: The left side portrays ILO, and the right side demonstrates how this inspire the training of a family of generative models with ILO-RTIL with parameters sharing.

is taken to be  $\alpha^k = \{\alpha'\}_k \cdot \mathbf{1}$  where  $\mathbf{1}$  is the vector of all ones and  $\{\alpha'\}_k$  is the  $k$ -th entry of the vector  $\alpha'$ . Note this leads to each channel being weighted equally during training. This process can be depicted in the appendix Figure 12.

## 4 Experiments

We observe that Regularized Training of Intermediate Layers is not tied to any specific architecture or training procedure, and while, until this point, we have only presented it on two-layer networks for easiness of exposition, in this section we demonstrate its successful application on two state of the art architectures on different imaging recovery problems. Specifically, we conduct extensive experiments comparing RTIL versus vanilla training for compressed sensing, inpainting, and super-resolution, and for two different inverse methods Multi-Code GAN Prior (Section 2.3) and Intermediate Layer Optimization (ILO) (Section 2.2) to demonstrate the effectiveness of our method. The generative model architecture used for the mGANprior is PGGAN [17] and for ILO is styleGAN-2 [19]. All models were trained on FFHQ data set [18] and tested on CelebA-HQ dataset [17], at an image size of  $256 \times 256 \times 3$ . The choice of architectures were based on the experimental section of the original ILO [7] and mGANprior [10] papers. Refer to the appendix for the architecture details for training networks using RTIL, as well as hyperparameters chosen for inversion methods.

For all experiments, compressed sensing use partial circulant measurement matrices with random signs [7], inpainting the pixels are missing at random, and down-sample factor corresponds to how much the height and width of the original image was reduced to.

### 4.1 Results ILO-RTIL

Results in this section correspond to Figure 6, where the results are average over three test sets of 12 images

randomly sampled from CelebA-HQ.

Compressed Sensing - ILO-RTIL demonstrates an increase in reconstruction performance across each under-sampling regime. The largest increase performance with respect to PSNR occur at 25% (1.28 dB), 15% (1.59 dB), and 10% (1.3 dB's) measurements. For qualitative results please refer to Figure 2. Inpainting-ILO-RTIL demonstrates in increase in reconstruction performance with 4 out of the 5 sampling regimes. There is increase in PSNR at 50% (1.88 dB), 25% (1.59 dB's), 15% (.94 db's), and 5% (.29 db) of observed pixels. At 1% of observed pixels there is a decrease in performance in reconstruction of .5 dB's, but the error bars overlap each other indicating there is no significant improvement. For qualitative results please refer to Figure 7. Super-Resolution - ILO-RTIL shows a slight increase in performance over the entire measurement regime compared to ILO, the most significant occurs at  $\frac{1}{4}$  downsampling factor where on average the increase in reconstruction is .77 dB's and the 95% error bars are separated. All other sampling regime achieve comparable performance between ILO-RTIL and ILO. For qualitative results please refer to the appendix Figure 16.

### 4.2 Results RTIL-Multi-Code

Results in this section correspond to Figure 7, where the results are average over five test sets of 12 images randomly sampled from CelebA-HQ. All experiments use  $N = 20$  latent codes. Compressed Sensing - mGANprior-RTIL has a significant improvement in reconstruction performance over mGANprior. For each under-sampling ratio our method increases performance by at least 1.6 dB's, which clearly separates the error bars. On the other hand, at 1% of measurements where both methods achieve the similar performance, which can be seen by overlapping error bars. For qualitative results refer to Figure 3. Inpainting-mGANprior-RTIL demonstrates a significant improvement in reconstructing over mGANprior clearly being

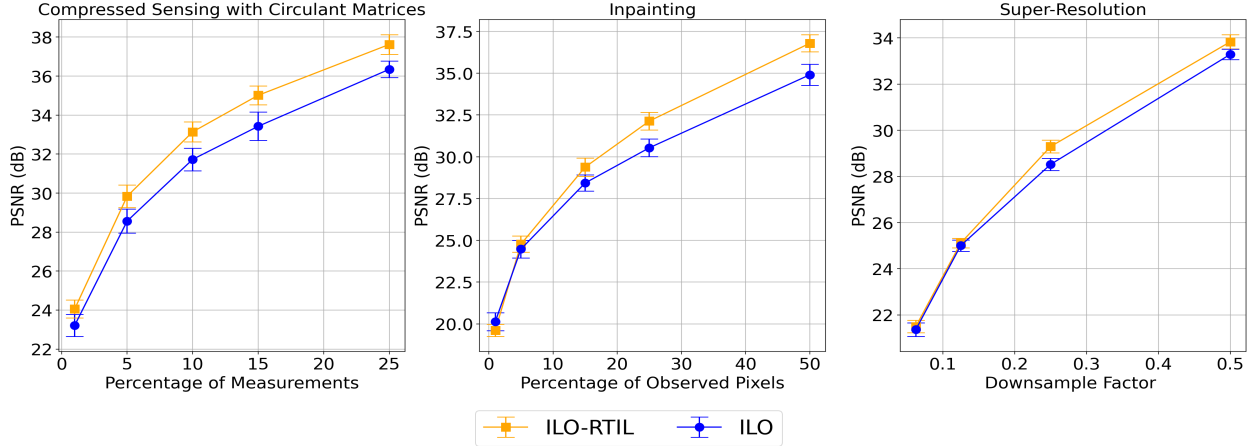


Figure 6: Performance of ILO-RTIL and vanilla trained ILO for Compressed sensing, inpainting, and super resolution for various under-sampling ratios. ILO-RTIL increases performances or ties for each under-sampling ratio with respect to PSNR across each inverse problems compared to ILO. The vertical bars indicate 95% confidence intervals.

able the error bars. Our method yields a increase in performance with respect to PSNR of 2.5 dB’s at 50%, 2.23 dB’s 30%, 1.99 dB’s at 20%, and 1.58 dB’s at 10% observed pixels. For 1% of observed pixels these both methods yield similar results. Lastly, qualitative results can be seen on Figure 15. Super-Resolution-mGAN-RTIL show substantial improvement with image reconstruction at downsampling factor of  $\frac{1}{2}$  and  $\frac{1}{4}$ , increase of 2.25 db’s and 1.51 dB’s respectively. However, at  $\frac{1}{16}$  down-sampling factor mGAN out performs RTIL-mGAN slightly, but within the error bars. For qualitative results please refer to the appendix Figure 17.

### 4.3 Ablation Study

This section provides two ablations studies, comparing vanilla training versus RTIL for each intermediate layer trained using ILO-RTIL and mGANprior-RTIL. Each experiment was test on 5 images sampled randomly from CelebA-HQ.

#### 4.3.1 ILO-RTIL

All results refer to Figure 8, recall Figure 5 and Algorithm 1 for notation,  $z_0$  refers to optimizing over the initial latent vector [6],  $z_1$  denotes sequentially optimizing over the first two layers, and so until representation error  $z_4$ .

Compressed Sensing - Overall, optimizing up to  $z_4$  achieves the best performance for ILO-RTIL and ILO, in most under-sampling ratio’s it outperforms and at worst ties compared to other intermediate optimization layers. Comparing ILO-RTIL to ILO,

there is increase in reconstruction performance on average across each under-sampling for  $z_4$  of 1.41 dB’s,  $z_3$  .81 dB’s,  $z_2$  .4 dB’s, and  $z_1$  .86 dB’s. Inpainting-Refer to appendix for inpainting results in Figure 8.

#### 4.3.2 mGANprior-RTIL

Compressed Sensing - mGANprior-RTIL outperformed vanilla mGANprior in each optimization setting using  $N = \{1, 10, 20\}$ , marginal at  $N = 1$ , but more noticeable at  $N = \{10, 20\}$ . Overall  $N = 20$  achieves the best performance for both mGANprior and mGANprior-RTIL training across each under-sampling regime. As well as mGANprior-RTIL increases performance on average across all the under-sampling experiments with  $N = 10$  compared to  $N = 20$  with mGANprior Inpainting-Refer to appendix for inpainting results in Figure 19.

## 5 Theoretical Model for Compressed Sensing with RTIL

In this section, we examine a simple theoretical model for compressive sensing with RTIL. To provide the most easily understandable context, we consider the case of a generative model given by a two-layer linear neural network. Further, we consider the case where the generative model is trained in a supervised manner, and we consider the regime of infinite training data. The supervised setting allows us to avoid discussing the different methods for learning generative models, and working in the infinite data regime we avoid statistical estimation errors.

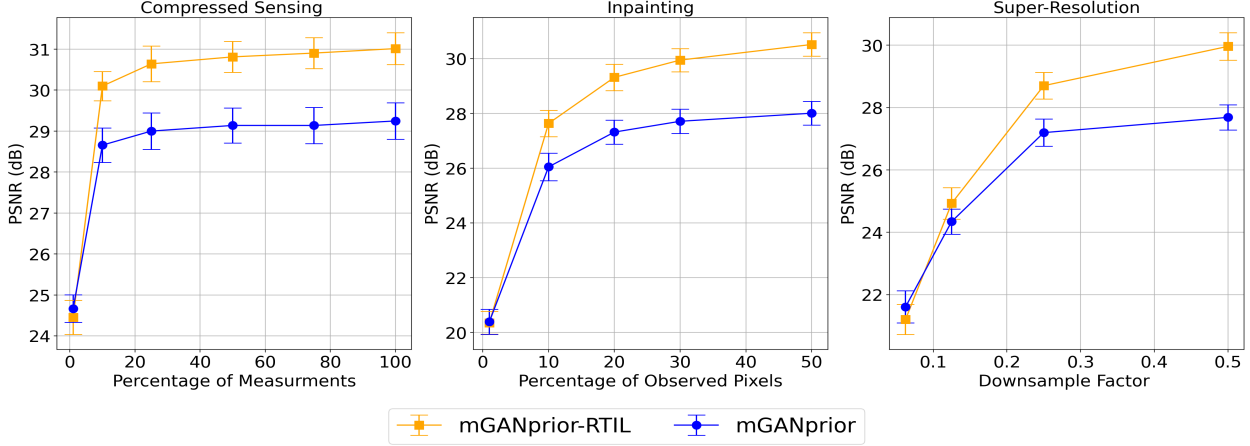


Figure 7: Performance of mGANprior-RTIL and vanilla trained mGAN for compressed sensing, inpainting, and super resolution for various under-sampling ratios. mGAN-RTIL increases performances over vanilla mGAN with respect to PSNR over each under-sampling ratio by a noticeable margin, except for super-resolution problems at low under-sampling ratio's. The vertical bars indicate 95% intervals.

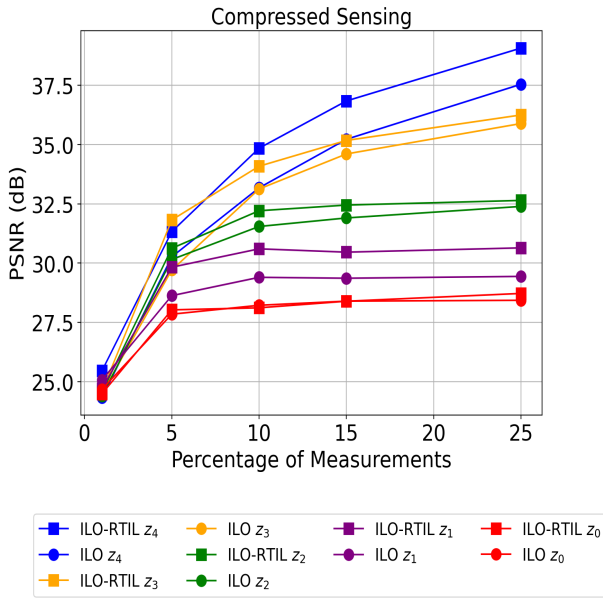


Figure 8: Comparing ILO-RTIL to ILO optimizing over various number of intermediate layers.

We assume that the true signal distribution is given by  $x = G^*(z_0, z_1) = W_1^*(W_0^*z_0 + z_1)$ , where  $G^* : \mathbb{R}^{n_0} \times \mathbb{R}^{n_1} \rightarrow \mathbb{R}^{n_d}$ ,  $z_0 \sim \mathcal{N}(0, I_{n_0})$  and  $z_1 \sim \mathcal{N}(0, I_{n_1})$  drawn independently, and where  $W_1^* \in \mathbb{R}^{n_d \times n_1}$  and  $W_0^* \in \mathbb{R}^{n_1 \times n_0}$ . We moreover assume that  $n_0 < n_1 < n_d$ , and  $W_0^*, W_1^*$  are full rank. We furthermore assume that  $W_0^*$  is known but that  $W_1^*$  is unknown.

## 5.1 Training the Models

We consider the training of two generative models. The first model is analogous to vanilla GAN training without RTIL. In it,  $G^{\text{Van}}(z_0) = W_1^{\text{Van}}(W_0^*z_0)$ . The second model is analogous to GAN training with RTIL. In it,  $\tilde{G}^{\text{RTIL}}(z_0, z_1) = W_1^{\text{RTIL}}(W_0^*z_0 + z_1)$ .

Training each model consists of estimating  $W_1^{\text{Van}}$  and  $W_1^{\text{RTIL}}$  under a least squares loss. As we consider the idealized regime of infinite training data, we obtain the following estimates:

$$W_1^{\text{Van}} \in \arg \min_{W_1 \in \mathbb{R}^{n_d \times n_1}} \mathbb{E}_{z_0, z_1} \|G^*(z_0, z_1) - W_1 W_0^* z_0\|_2^2, \quad (2)$$

and

$$W_1^{\text{RTIL}} \in \arg \min_{W_1 \in \mathbb{R}^{n_d \times n_1}} \mathbb{E}_{z_0, z_1} \|G^*(z_0, z_1) - W_1(W_0^*z_0 + z_1)\|_2^2. \quad (3)$$

The next lemma is a simple consequence of the property of the Gaussian distribution.

**Lemma 5.1.** *Let  $W_1^{\text{Van}}$  satisfy in (2) then  $W_1^{\text{Van}}W_0^* = W_1^*W_0^*$ . Moreover, there exists a unique  $W_1^{\text{RTIL}}$  solution of (3), given by  $W_1^{\text{RTIL}} = W_1^*$ .*

While the above lemma shows that  $W_1^{\text{Van}}$  will equal  $W_1^*$  on the range of  $W_0^*$ , its behavior on the space orthogonal to the range of  $W_0^*$  depends on how (2) is solved. To simplify the discussion below we will consider  $W_1^{\text{Van}}$  to be the minimum (Frobenius) norm solution of (2).



## 5.2 Compressed Sensing

We next analyze the compressed sensing problem with the trained generative models. Let  $x^* = G^*(z_0^*, z_1^*)$  be an unknown signal, where  $z_0^* \sim \mathcal{N}(0, I_{n_0})$  and  $z_1^* \sim \mathcal{N}(0, I_{n_1})$ . We consider the problem of recovering  $x^*$  given compressed linear measurements  $y = Ax^* \in \mathbb{R}^m$  where  $n_1 \leq m < n_d$ . When using the base model  $G^{\text{Van}}$  and the higher dimensional model  $\tilde{G}^{\text{Van}}$ , we solve

$$\begin{aligned} z_0^{\text{van}} &= \arg \min_{\hat{z}_0 \in \mathbb{R}^{n_0}} \|y - AG^{\text{Van}}(\hat{z}_0)\|_2^2, \\ z_1^{\text{van}} &= \arg \min_{\hat{z}_1 \in \mathbb{R}^{n_1}} \|y - A\tilde{G}^{\text{Van}}(z_0^{\text{van}}, \hat{z}_1)\|_2^2. \end{aligned}$$

We denote with  $\tilde{G}^{\text{Van}}$  the vanilla model trained with (2), where  $z_1$  is introduced as an intermediate variable,  $\tilde{G}^{\text{Van}}(z_0, z_1) = W_1^{\text{Van}}(W_0^* z_0 + z_1)$ . When using the model  $\tilde{G}^{\text{RTIL}}$  trained with RTIL, we solve

$$\begin{aligned} z_0^{\text{rtil}} &= \arg \min_{\hat{z}_0 \in \mathbb{R}^{n_0}} \|y - A\tilde{G}^{\text{RTIL}}(\hat{z}_0, 0)\|_2^2, \\ z_1^{\text{rtil}} &= \arg \min_{\hat{z}_1 \in \mathbb{R}^{n_1}} \|y - A\tilde{G}^{\text{RTIL}}(z_0^{\text{rtil}}, \hat{z}_1)\|_2^2. \end{aligned}$$

Moreover, we take  $z_1^{\text{rtil}}$  to be the minimum norm solution. As shown in the proof  $z_0^{\text{van}}$  and  $(z_0^{\text{rtil}}, z_1^{\text{rtil}})$  are unique. Notice that  $(z_0^{\text{van}}, z_1^{\text{van}})$  and  $(z_0^{\text{rtil}}, z_1^{\text{rtil}})$  correspond to the latent vector and intermediate layer variables obtained applying the ILO Algorithm 1 with inputs  $\{\tilde{G}^{\text{Van}}, A, y\}$  and  $\{\tilde{G}^{\text{RTIL}}, A, y\}$  respectively.

The following lemma quantifies the reconstruction errors made by using the two generative models.

**Lemma 5.2.** *Assume that  $W_0^*, W_1^*$  are full rank. Let  $W_1^{\text{Van}}$  be the minimum norm solution of (2) and  $W_1^{\text{RTIL}}$  be the solution of (3). Let  $A \in \mathbb{R}^{m \times n_d}$  with i.i.d.  $\mathcal{N}(0, 1)$  entries. Then with probability 1*

$$\begin{aligned} &\mathbb{E}_{z_0^*, z_1^*} [\|G^*(z_0^*, z_1^*) - \tilde{G}^{\text{Van}}(z_0, z_1)\|^2] \\ &\geq \max_{h \in \text{range}(W_0^*)^\perp} \|(I_{n_d} - \mathcal{P}_{W_1^* W_0^*}) W_1^* h\|_2^2 > 0 \end{aligned} \quad (4)$$

and

$$\mathbb{E}_{z_0^*, z_1^*} [\|G^*(z_0^*, z_1^*) - \tilde{G}^{\text{RTIL}}(\tilde{z}_0, \tilde{z}_1)\|^2] = 0. \quad (5)$$

The above results illustrate why training generative models using RTIL can enable better compressed sensing performance. In the simplified setting of a two-layer linear neural network trained in a supervised manner with a known first layer and in the infinite data regime, we see that the lower dimensional generative model incurs error in the second layer's weights in the orthogonal complement of the range of the first layer. This results in an increase in the reconstruction error when solving compressed sensing.

## 6 Conclusion

We have introduced a principle for training GANs that are intended to be used for solving inverse problems. That principle states that if the inversion algorithm optimizes over intermediate layers of the network, then during training the network should be regularized in those layers. We instantiate this principle for two recent and successful optimization algorithms, Intermediate Layer Optimization [7] and the Multi-Code Prior [10]. For both of these algorithm, we devise a new GAN training algorithm. Empirically, we show our trained GANs allow better reconstruction in compressed sensing, inpainting, and super resolution across multiple under-sampling regimes, when compared to GANs trained in a vanilla manner. We note that our methodology only applies in the case of inversion methods that optimize over intermediate layers. However, there has been multiple competitive methods of this form published recently, each of which we show can benefit from this approach. Tools like those proposed in this paper, provided sufficient computational resources, may allow these methods to be even more competitive in real-world applications.

## References

- [1] Ardizzone, Lynton, Kruse, Jakob, Rother, Carsten, & Köthe, Ullrich. 2019. Analyzing Inverse Problems with Invertible Neural Networks. *In: International Conference on Learning Representations*.
- [2] Arjovsky, Martin, Chintala, Soumith, & Bottou, Léon. 2017. Wasserstein generative adversarial networks. *Pages 214–223 of: International conference on machine learning*. PMLR.
- [3] Asim, Muhammad, Daniels, Max, Leong, Oscar, Ahmed, Ali, & Hand, Paul. 2020. Invertible generative models for inverse problems: mitigating representation error and dataset bias. *Pages 399–409 of: International Conference on Machine Learning*. PMLR.
- [4] Athar, ShahRukh, Burnaev, Evgeny, & Lempitsky, Victor. 2018. Latent convolutional models. *arXiv preprint arXiv:1806.06284*.
- [5] Bojanowski, Piotr, Joulin, Armand, Lopez-Pas, David, & Szlam, Arthur. 2018. Optimizing the Latent Space of Generative Networks. *Pages 600–609 of: International Conference on Machine Learning*. PMLR.
- [6] Bora, Ashish, Jalal, Ajil, Price, Eric, & Dimakis, Alexandros G. 2017. Compressed sensing using generative models. *Pages 537–546 of: International Conference on Machine Learning*. PMLR.
- [7] Daras, Giannis, Dean, Joseph, Jalal, Ajil, & Dimakis, Alex. 2021. Intermediate Layer Optimization for Inverse Problems using Deep Generative Models. *Pages 2421–2432 of: Meila, Marina, & Zhang, Tong (eds), Proceedings of the 38th International Conference on Machine Learning, ICML 2021, 18–24 July 2021, Virtual Event*. Proceedings of Machine Learning Research, vol. 139. PMLR.
- [8] Dhar, Manik, Grover, Aditya, & Ermon, Stefano. 2018. Modeling sparse deviations for compressed sensing using generative models. *Pages 1214–1223 of: International Conference on Machine Learning*. PMLR.
- [9] Goodfellow, Ian, Pouget-Abadie, Jean, Mirza, Mehdi, Xu, Bing, Warde-Farley, David, Ozair, Sherjil, Courville, Aaron, & Bengio, Yoshua. 2014. Generative Adversarial Nets. *In: Ghahramani, Z., Welling, M., Cortes, C., Lawrence, N., & Weinberger, K. Q. (eds), Advances in Neural Information Processing Systems*, vol. 27. Curran Associates, Inc.
- [10] Gu, Jinjin, Shen, Yujun, & Zhou, Bolei. 2020 (June). Image Processing Using Multi-Code GAN Prior. *In: Proceedings of the IEEE/CVF Conference on Computer Vision and Pattern Recognition (CVPR)*.
- [11] Gulrajani, Ishaan, Ahmed, Faruk, Arjovsky, Martín, Dumoulin, Vincent, & Courville, Aaron C. 2017. Improved Training of Wasserstein GANs. *In: NIPS*.
- [12] Hand, Paul, Leong, Oscar, & Voroninski, Vlad. 2018. Phase Retrieval Under a Generative Prior. *In: Bengio, S., Wallach, H., Larochelle, H., Grauman, K., Cesa-Bianchi, N., & Garnett, R. (eds), Advances in Neural Information Processing Systems*, vol. 31. Curran Associates, Inc.
- [13] Helminger, Leonhard, Bernasconi, Michael, Djelouah, Abdelaziz, Gross, Markus, & Schroers, Christopher. 2021. Generic Image Restoration With Flow Based Priors. *Pages 334–343 of: Proceedings of the IEEE/CVF Conference on Computer Vision and Pattern Recognition*.
- [14] Hussein, Shady Abu, Tirer, Tom, & Giryes, Raja. 2020. Image-adaptive GAN based reconstruction. *Pages 3121–3129 of: Proceedings of the AAAI Conference on Artificial Intelligence*, vol. 34.
- [15] Jalal, Ajil, Karmalkar, Sushrut, Dimakis, Alexandros G, & Price, Eric. 2021a. Instance-Optimal Compressed Sensing via Posterior Sampling. *arXiv preprint arXiv:2106.11438*.
- [16] Jalal, Ajil, Arvinte, Marius, Daras, Giannis, Price, Eric, Dimakis, Alexandros G, & Tamir, Jonathan I. 2021b. Robust Compressed Sensing MRI with Deep Generative Priors. *arXiv preprint arXiv:2108.01368*.
- [17] Karras, Tero, Aila, Timo, Laine, Samuli, & Lehtinen, Jaakko. 2018. Progressive Growing of GANs for Improved Quality, Stability, and Variation. *In: International Conference on Learning Representations*.
- [18] Karras, Tero, Laine, Samuli, & Aila, Timo. 2019. A style-based generator architecture for generative adversarial networks. *Pages 4401–4410 of: Proceedings of the IEEE/CVF Conference on Computer Vision and Pattern Recognition*.
- [19] Karras, Tero, Laine, Samuli, Aittala, Miika, Hellsten, Janne, Lehtinen, Jaakko, & Aila, Timo. 2020. Analyzing and improving the image quality of stylegan. *Pages 8110–8119 of: Proceedings of the*

- IEEE/CVF Conference on Computer Vision and Pattern Recognition.*
- [20] Kelkar, Varun A, Bhadra, Sayantan, & Anastasio, Mark A. 2021. Compressible latent-space invertible networks for generative model-constrained image reconstruction. *IEEE Transactions on Computational Imaging*, **7**, 209–223.
- [21] Kingma, Diederik P., & Ba, Jimmy. 2015. Adam: A Method for Stochastic Optimization. In: Bengio, Yoshua, & LeCun, Yann (eds), *3rd International Conference on Learning Representations, ICLR 2015, San Diego, CA, USA, May 7-9, 2015, Conference Track Proceedings.*
- [22] Ma, Jianwei, & Le Dimet, Francois-Xavier. 2009. Deblurring from highly incomplete measurements for remote sensing. *IEEE transactions on geoscience and remote sensing*, **47**(3), 792–802.
- [23] Mardani, Morteza, Gong, Enhao, Cheng, Joseph Y, Vasanaawala, Shreyas S, Zaharchuk, Greg, Xing, Lei, & Pauly, John M. 2018. Deep generative adversarial neural networks for compressive sensing MRI. *IEEE transactions on medical imaging*, **38**(1), 167–179.
- [24] Menon, Sachit, Damian, Alexandru, Hu, Shijia, Ravi, Nikhil, & Rudin, Cynthia. 2020. Pulse: Self-supervised photo upsampling via latent space exploration of generative models. *Pages 2437–2445 of: Proceedings of the ieee/cvf conference on computer vision and pattern recognition.*
- [25] Mosser, Lukas, Dubrulle, Olivier, & Blunt, Martin J. 2020. Stochastic seismic waveform inversion using generative adversarial networks as a geological prior. *Mathematical Geosciences*, **52**(1), 53–79.
- [26] Pan, Xingang, Dai, Bo, Liu, Ziwei, Loy, Chen Change, & Luo, Ping. 2021. Do 2D {GAN}s Know 3D Shape? Unsupervised 3D Shape Reconstruction from 2D Image {GAN}s. In: *International Conference on Learning Representations.*
- [27] Ramzi, Zaccharie, Rémy, Benjamin, Lanusse, Francois, Starck, Jean-Luc, & Ciuciu, Philippe. 2020. Denoising Score-Matching for Uncertainty Quantification in Inverse Problems. *arXiv preprint arXiv:2011.08698.*
- [28] Shamshad, Fahad, Hanif, Asif, & Ahmed, Ali. 2019. Subsampled Fourier ptychography via pre-trained invertible and untrained network priors.
- [29] Smedemark-Margulies, Niklas, Park, Jung Yeon, Daniels, Max, Yu, Rose, van de Meent, Jan-Willem, & Hand, Paul. 2021. Generator Surgery for Compressed Sensing. *arXiv preprint arXiv:2102.11163.*
- [30] Song, Yang, & Ermon, Stefano. 2019. Generative modeling by estimating gradients of the data distribution. *arXiv preprint arXiv:1907.05600.*
- [31] Song, Yang, & Ermon, Stefano. 2020. Improved techniques for training score-based generative models. *arXiv preprint arXiv:2006.09011.*
- [32] Song, Yang, Sohl-Dickstein, Jascha, Kingma, Diederik P, Kumar, Abhishek, Ermon, Stefano, & Poole, Ben. 2020. Score-based generative modeling through stochastic differential equations. *arXiv preprint arXiv:2011.13456.*
- [33] Whang, Jay, Lindgren, Erik, & Dimakis, Alex. 2021a. Composing Normalizing Flows for Inverse Problems. *Pages 11158–11169 of: International Conference on Machine Learning.* PMLR.
- [34] Whang, Jay, Lei, Qi, & Dimakis, Alex. 2021b. Solving Inverse Problems with a Flow-based Noise Model. *Pages 11146–11157 of: International Conference on Machine Learning.* PMLR.
- [35] Zhang, Richard, Isola, Phillip, Efros, Alexei A, Shechtman, Eli, & Wang, Oliver. 2018. The Unreasonable Effectiveness of Deep Features as a Perceptual Metric. In: *CVPR.*

## A Appendix

Code provided in supplementary folder. Computational requirements for this paper are two NVIDIA 2080 Ti GPU: training StyleGAN2 uses both GPU’s and one GPU for inversion, training PGGAN requires one GPU and one for inversion.

### A.1 RTIL-ILO Training Details

All experiments for ILO inversion method used StyleGAN2 architecture [19], both vanilla and RTIL models were trained for 700,000 iterations using the same training parameters, i.e., learning rate, batch size, and regularization updates. Below table 1 outlines the macroscopic view of the StlyeGAN2 architecture. Please refer StlyeGAN2 paper [19] for more architecture details, between each convolutional layer there normalization operation called weight demodulation. During training for RTIL the distribution was induced after each block in the network, which corresponds to a cells 2-6 in table 1 up to 4-th convolutional block.

All experiments for ILO inversion method used StyleGAN2 architecture [19], both vanilla and RTIL models were trained for 700,000 iterations using the same training parameters, i.e., learning rate, batch size, and regularization updates. Please refer to the code for more details on the training process and the StlyeGAN2 paper [19] for more details on the architecture. Below Table 1 outlines the macroscopic view of the StlyeGAN2 architecture, between each convolutional layer there is a normalization operation called weight demodulation. During training for RTIL the additional latent variables were added after each block in the network, which correspond to cells 2-6 in Table 1 up to 4-th convolutional block.

Table 1: StyleGan2 for image size  $256 \times 256 \times 3$

Generator		
Operation	Activation	Output Shape
Latent Vector	None	$512 \times 1 \times 1$
$8 \times$ MLP (Mapping Network)	LRelu	$512 \times 14$
Constant input	None	$512 \times 4 \times 4$
Conv $3 \times 3$	LRelu	$256 \times 4 \times 4$
Upsample	None	$256 \times 8 \times 8$
Conv $3 \times 3$	LRelu	$256 \times 8 \times 8$
Conv $3 \times 3$	LRelu	$256 \times 8 \times 8$
Upsample	None	$256 \times 16 \times 16$
Conv $3 \times 3$	LRelu	$256 \times 16 \times 16$
Conv $3 \times 3$	LRelu	$256 \times 16 \times 16$
Upsample	None	$256 \times 32 \times 32$
Conv $3 \times 3$	LRelu	$256 \times 32 \times 32$
Conv $3 \times 3$	LRelu	$256 \times 32 \times 32$
Upsample	None	$256 \times 64 \times 64$
Conv $3 \times 3$	LRelu	$256 \times 64 \times 64$
Conv $3 \times 3$	LRelu	$256 \times 64 \times 64$
Upsample	None	$128 \times 128 \times 128$
Conv $3 \times 3$	LRelu	$128 \times 128 \times 128$
Conv $3 \times 3$	LRelu	$128 \times 128 \times 128$
Upsample	None	$128 \times 256 \times 256$
Conv $3 \times 3$	LRelu	$64 \times 256 \times 256$
Conv $3 \times 3$	LRelu	$64 \times 256 \times 256$
Conv $1 \times 1$	Linear	$3 \times 256 \times 256$
<b>Trainable Parameters : 12,300,877</b>		



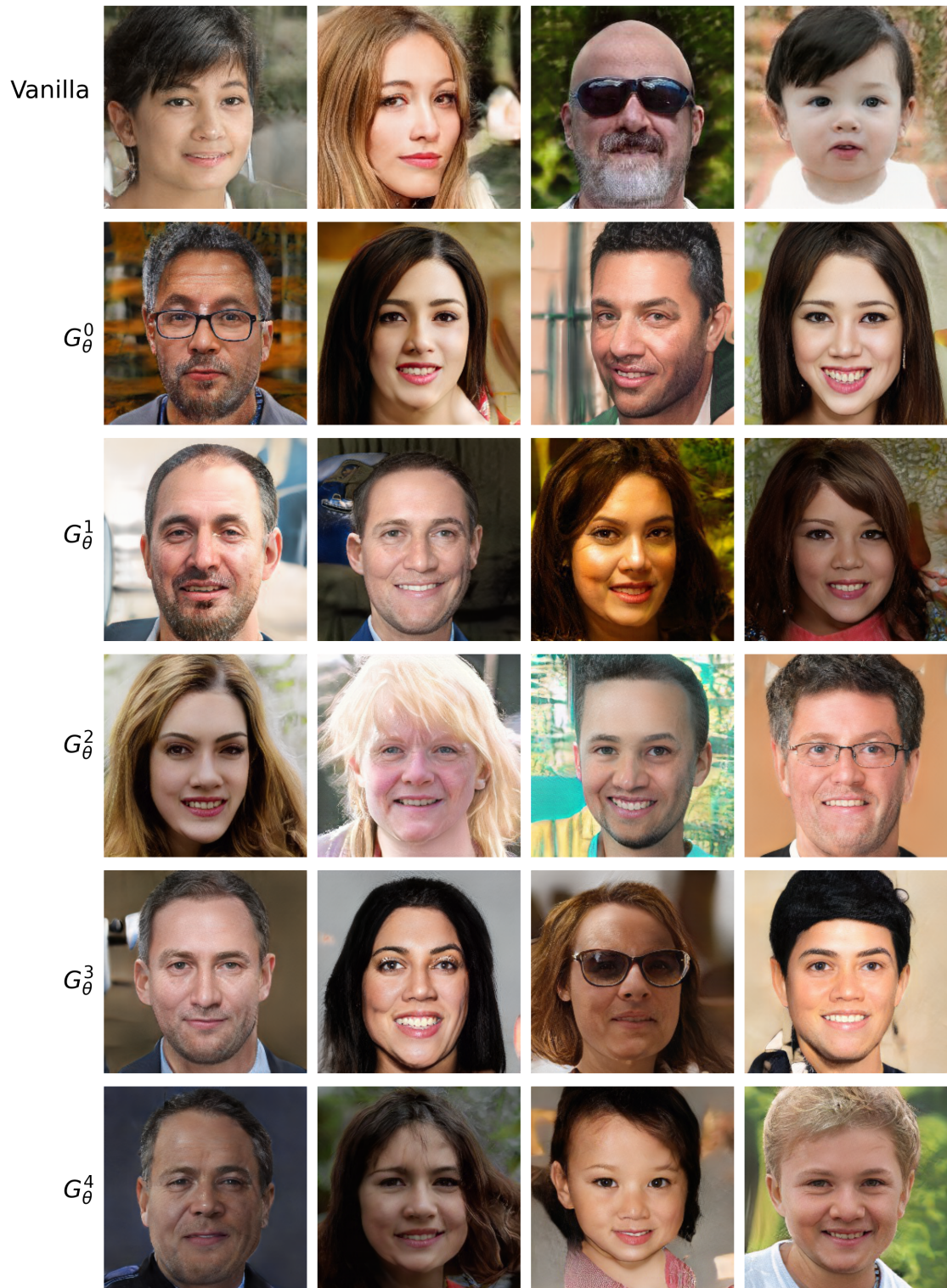


Figure 9: Samples from each of our trained generative models. Top row consist samples from vanilla trained StyleGAN2, then rows  $G_\theta^0 \cdots G_\theta^4$  are samples from family of generative models trained with RTIL.

## A.2 RTIL-mGANprior Training Details

All experiments for mGANprior inversion method used PGGAN Architecture [17], both vanilla and RTIL models were trained for 700,000 iterations and use the same training parameters, i.e., learning rate, batch size, and regularization updates. If interested please to refer to the code for more details. Below table 2 outlines the details of the PGGAN architecture. The intermediate latent variable were added after the 4-th block, which corresponds to the 4-th cell in Table 2.

Table 2: PGGAN for image size  $256 \times 256 \times 3$

<b>Generator</b>		
Operation	Activation	Output Shape
Latent Vector	None	$512 \times 1 \times 1$
Conv $4 \times 4$	LRelu	$256 \times 4 \times 4$
Conv $3 \times 3$	LRelu	$256 \times 4 \times 4$
Upsample	None	$256 \times 8 \times 8$
Conv $3 \times 3$	LRelu	$256 \times 8 \times 8$
Conv $3 \times 3$	LRelu	$256 \times 8 \times 8$
Upsample	None	$256 \times 16 \times 16$
Conv $3 \times 3$	LRelu	$256 \times 16 \times 16$
Conv $3 \times 3$	LRelu	$256 \times 16 \times 16$
Upsample	None	$256 \times 32 \times 32$
Conv $3 \times 3$	LRelu	$256 \times 32 \times 32$
Conv $3 \times 3$	LRelu	$256 \times 32 \times 32$
Upsample	None	$256 \times 64 \times 64$
Conv $3 \times 3$	LRelu	$128 \times 64 \times 64$
Conv $3 \times 3$	LRelu	$128 \times 64 \times 64$
Upsample	None	$128 \times 128 \times 128$
Conv $3 \times 3$	LRelu	$64 \times 128 \times 128$
Conv $3 \times 3$	LRelu	$64 \times 128 \times 128$
Upsample	None	$64 \times 256 \times 256$
Conv $3 \times 3$	LRelu	$64 \times 256 \times 256$
Conv $3 \times 3$	LRelu	$64 \times 256 \times 256$
Conv $1 \times 1$	Linear	$3 \times 256 \times 256$
<b>Trainable Parameters : 7,445,443</b>		

### A.3 Inversion Details for ILO

Hyper-parameters were tuned based on indications in the appendix of the ILO paper [7] and the official implementation. Specifically, learning rate and number of iterations per layer were tuned for compressed sensing, then the same configuration were used for inpainting and super-resolution. For experiments in Section 4.1 Figure 6 the configuration for the number of iterations per layer is  $\{2000, 1000, 1000, 1000, 2000\}$ . ILO-RTIL uses a learning rate that begins at .2 at the initial layer, then ramps up linearly and ramps down using a cosine scheduler, as proposed by [19]. As for ILO, each layer initialized with a learning rate of .1 then optimized independently using the same learning rate scheduler, which is proposed in official Github repository [7]. We choose the intermediate layer up to which optimize to, based on ablation study Section 4.3.1 Figure 8. Below we report the loss function used for each inverse problem in case of ILO-RTIL and RTIL:

- *Compressed Sensing* - Mean square error
- *Inpainting*- Equal weighted combination of mean square error and LPIPS [35] for sufficient number of measurements. Notice that with more than 50% missing pixels LPIPS did not help reconstruction performance.
- *Super-Resolution* - Equal weighted combination of mean square error and LPIPS for RTIL models, for vanilla trained models LPIPS was weighted more. This configuration demonstrated increase in performance for all under-sampling ratio's. Best performance occurred when MSE and LPIPS used same image dimensions, i.e no upsampling for the LPIPS loss. For more details refer to GitHub code.

### A.4 Inversion Details for mGANprior

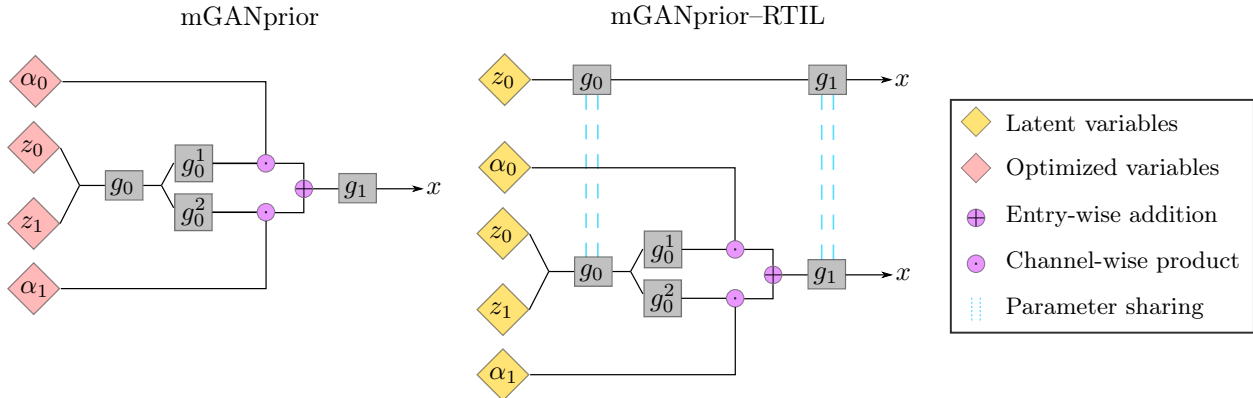


Figure 12: The left side portrays vanilla training for mGANprior, and the right side demonstrates RTIL. For mGANprior-RTIL this example with  $N = 2$  latent codes, where the top model trains a vanilla model analogous to model on the left, then parameter shares with the model below.

Hyper-parameters were tuned based on the Github repository [10] for Section 4.2 Figure 7, learning rate and the number of iterations were tuned for compressed sensing then reused for inpainting and super-resolution. mGANprior-RTIL uses Adam [21] optimizer initialized at learning rate of .1 and optimized for 2500 iterations. mGANprior uses SGD initialized at learning rate 1 and optimized for 2500 iterations, which is based on the official Github repository [10]. Empirically, the mGANprior [10] improvement in reconstruction saturated after  $N = 20$  latent codes. Moreover, for selecting which intermediate layer to optimize over for the vanilla model was determined by the ablation study in Figure 13. Below we report the loss function used for each inverse problem in case of mGANprior-RTIL and mGANprior

- *Compressed Sensing* - Mean square error loss for both methods.

- *Inpainting*- Mean square error plus  $l_1$  LPIPS regularization proposed by [10]. For mGANprior-RTIL the regularization term was  $\lambda = .1$  and for mGANprior  $\lambda = .5$ .
- *Super-Resolution* - Mean square error plus  $l_1$  LPIPS regularization proposed by [10] or mGANprior-RTIL the regularization term was scaled  $\lambda = .1$  and for mGANprior  $\lambda = .5$ . Best performance occurred when MSE and LPIPS used same image dimensions, i.e no upsampling for the LPIPS loss.

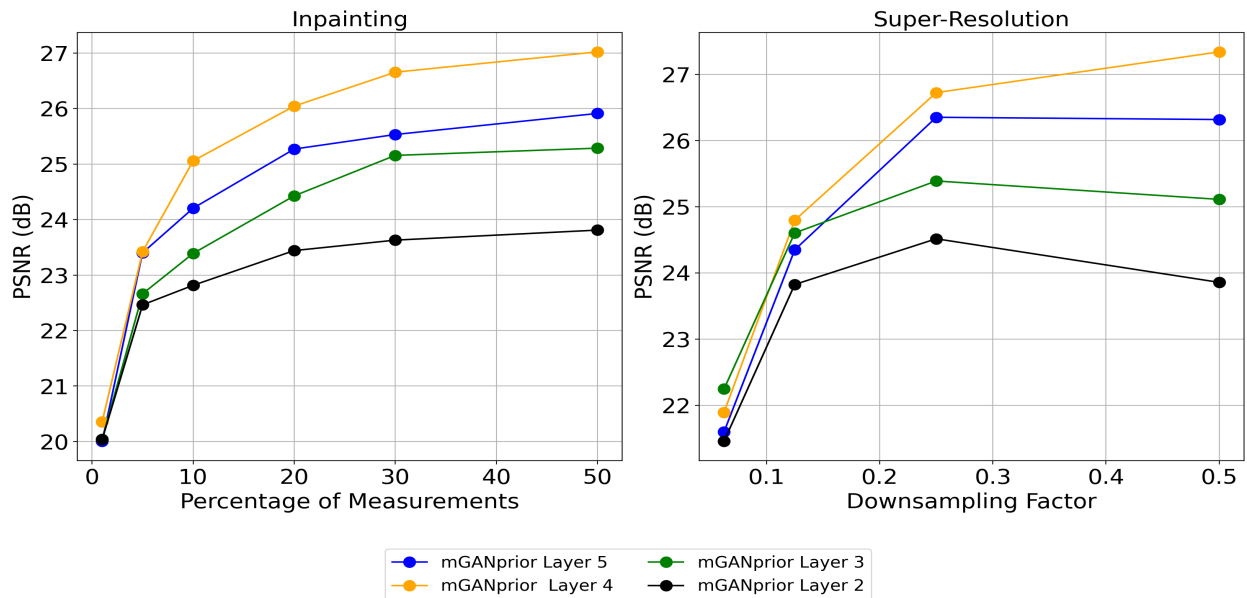


Figure 13: Effects on in-painting and super-resolution performance for various intermediate layer on validation set of 5 images.

## A.5 Inverse Problems Qualitative Results

### Inpainting



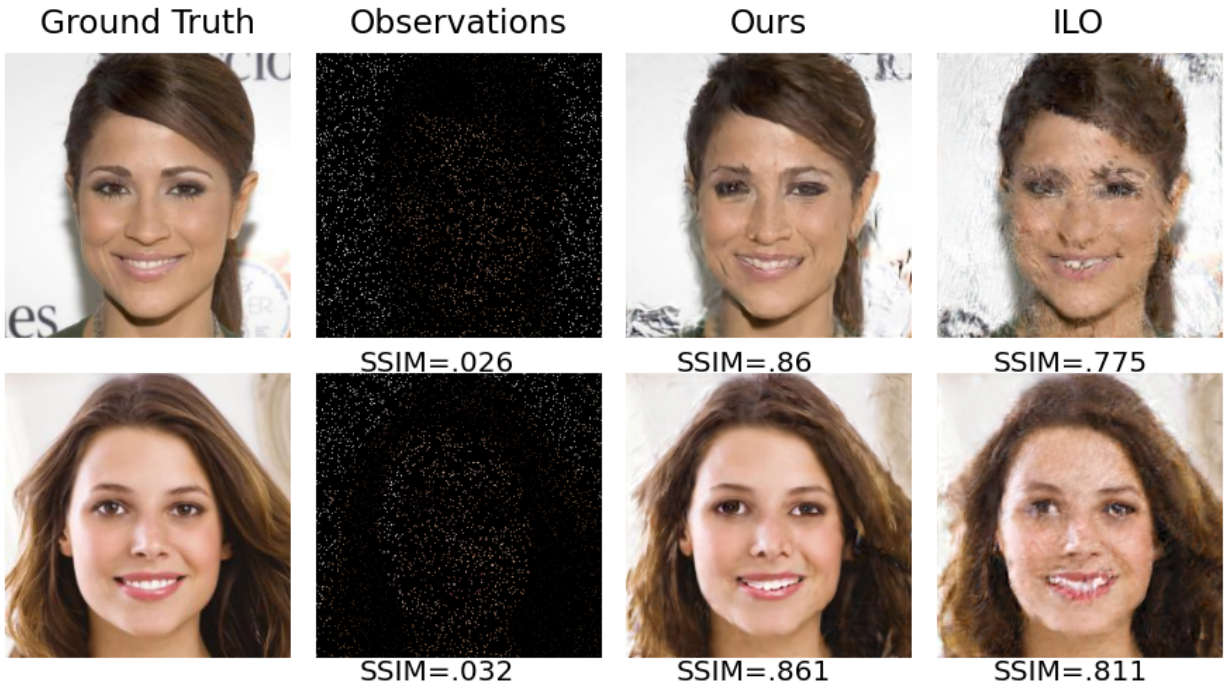


Figure 14: Qualitative comparison between our method ILO-RTIL and ILO for inpainting at 5% of observed pixels.

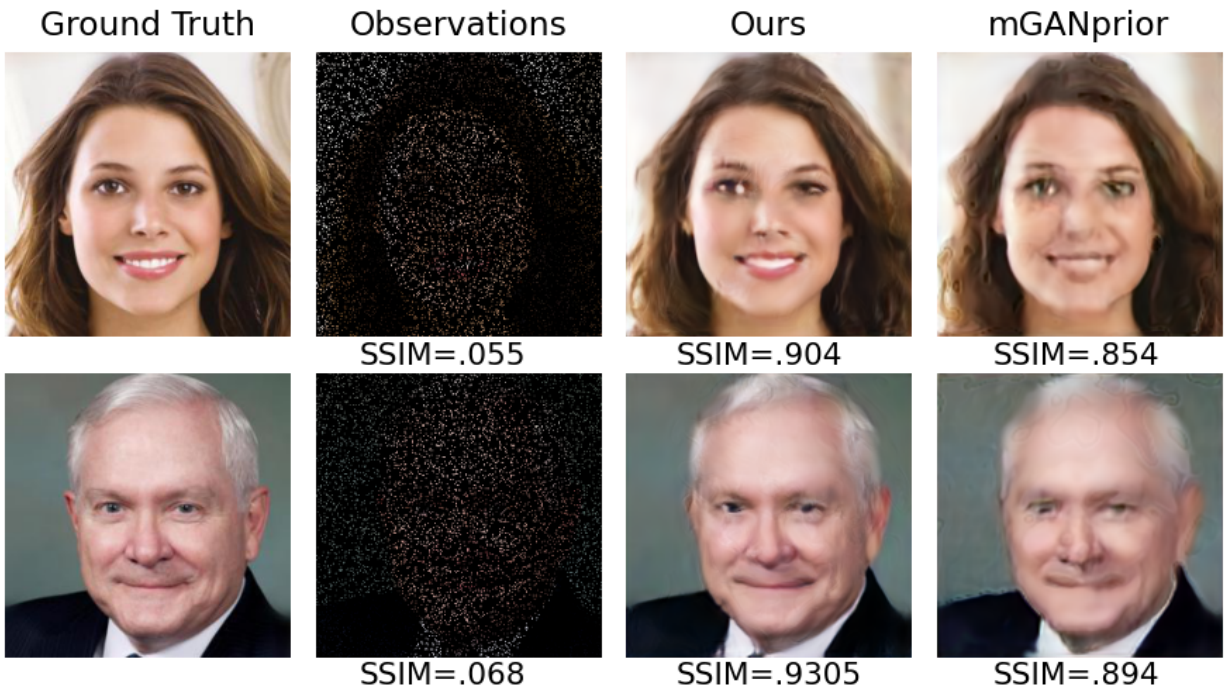


Figure 15: Qualitative comparison between our method mGANprior-RTIL and mGANprior for inpainting at 10% of observed pixels.

## Super-Resolution

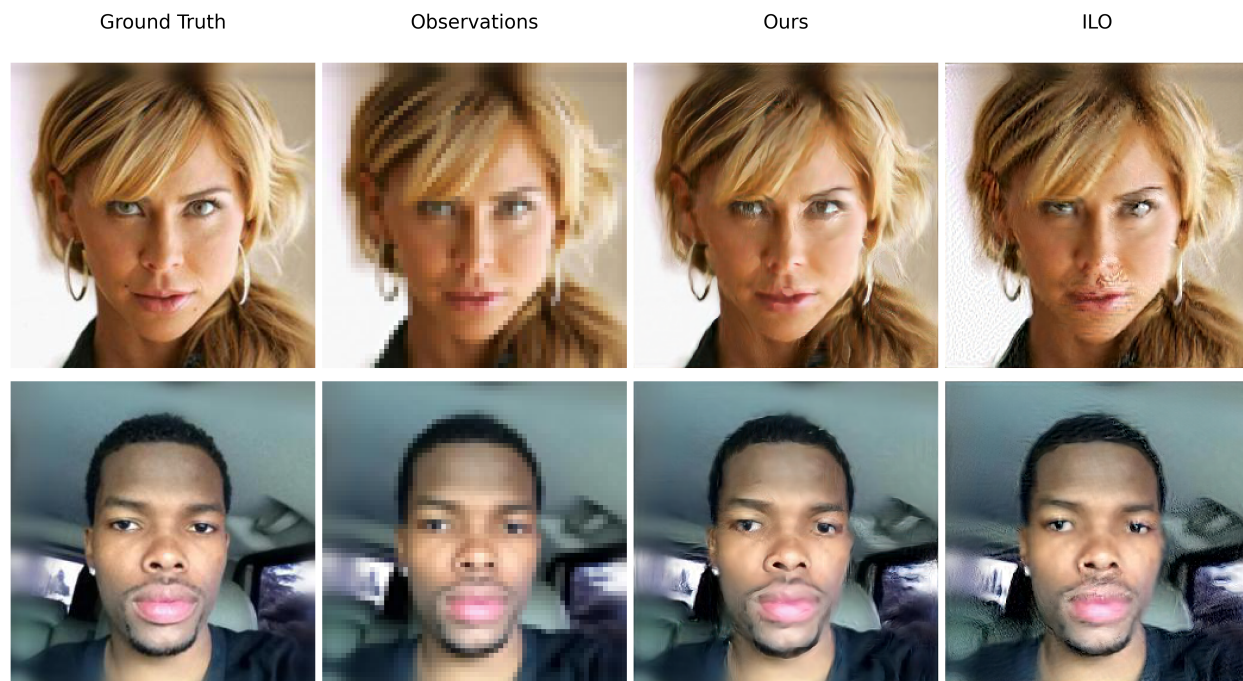


Figure 16: Comparison between ILO-RTIL to ILO for super-resolution LR 4x (Downsampling factor  $\frac{1}{4}$ )

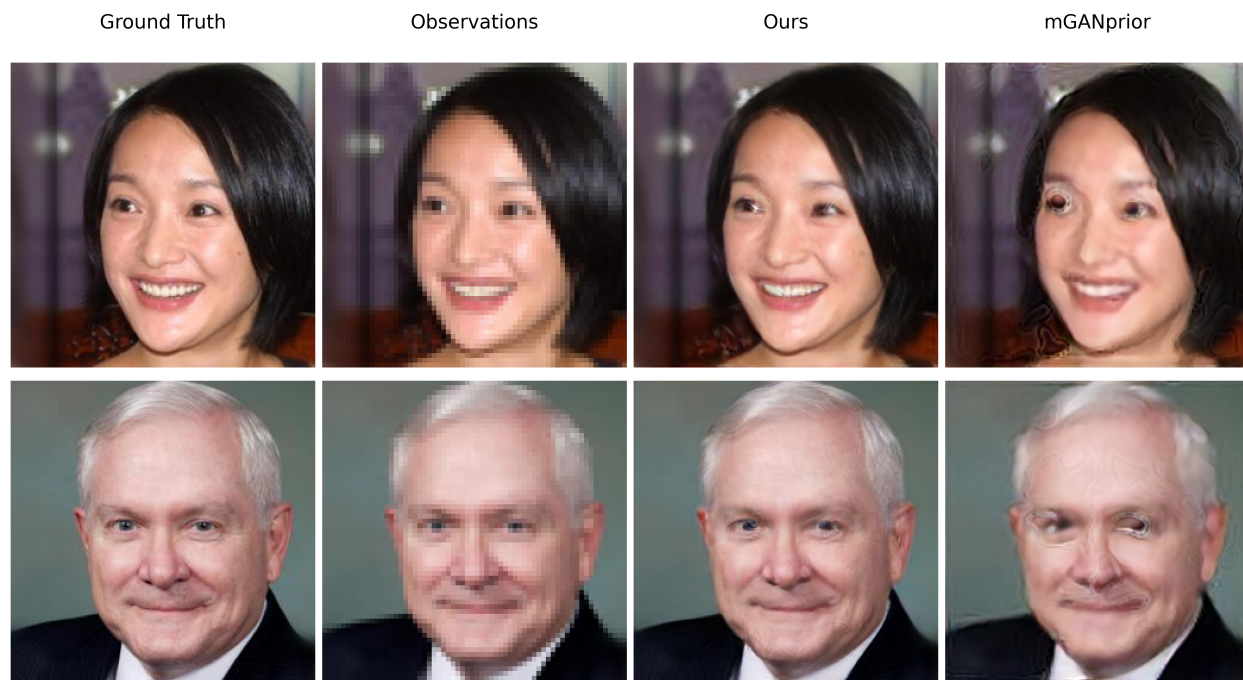


Figure 17: Comparison between mGANprior-RTIL to mGANprior for super-Resolution LR 4x (Downsampling factor  $\frac{1}{4}$ )

## A.6 Ablation

### A.6.1 ILO-Ablation

This section corresponds to Section 4.3.1, Figure 8, the configuration for each optimization setting go as:  $z_0 = \{2000\}$ ,  $z_1 = \{2000, 2000\}$ ,  $z_2 = \{2000, 1000, 2000\}$ ,  $z_3 = \{2000, 1000, 1000, 2000\}$ ,  $z_4 = \{2000, 1000, 1000, 1000, 2000\}$  iterations per layer.

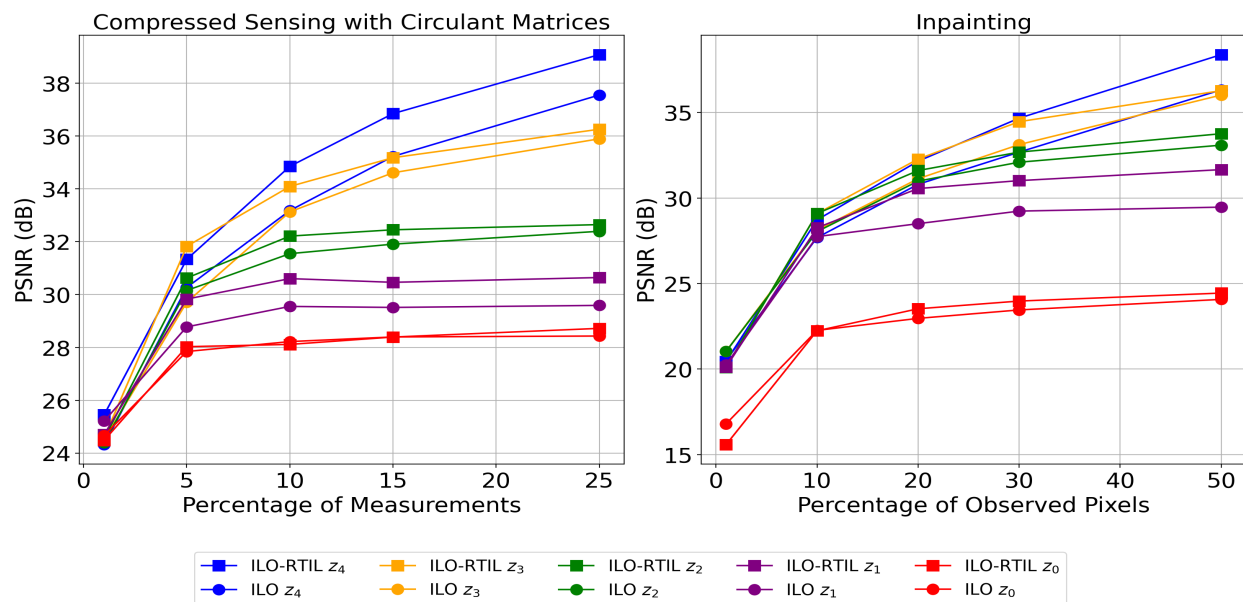


Figure 18: Comparing compressed sensing performance between ILO-RTIL and ILO for various number of intermediate layers.

### A.6.2 mGANprior-Ablation

This section corresponds to Section 4.3.2

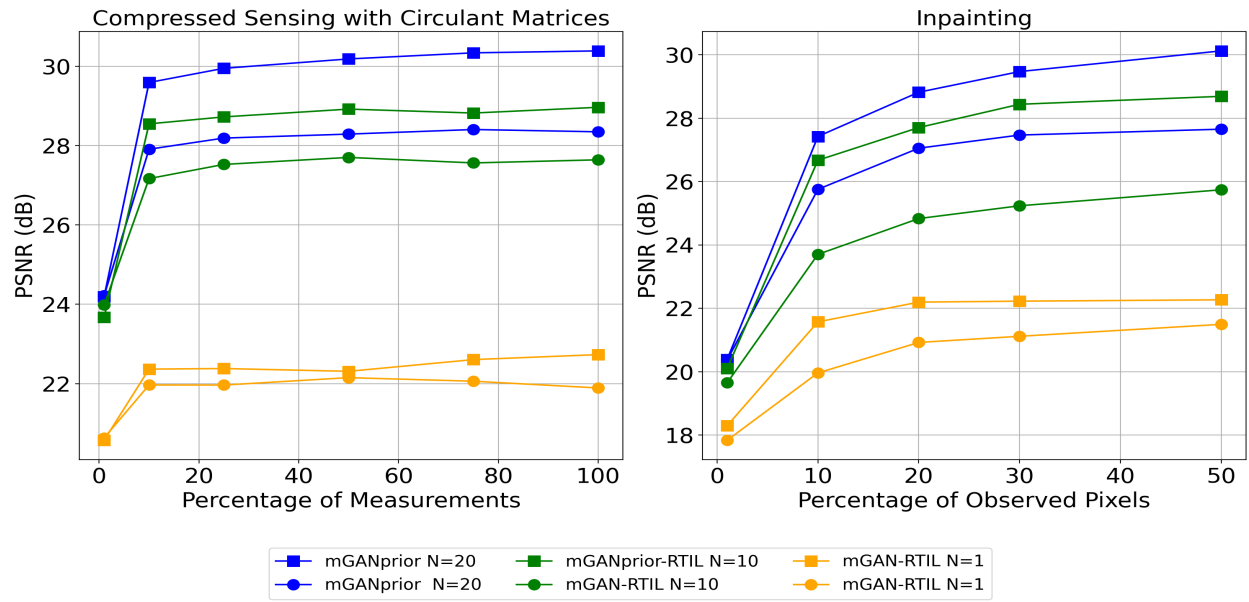


Figure 19: Comparing compressed sensing performance between mGANprior-RTIL and mGANprior for various number of latent codes.



## B Proof

*Proof of Lemma 5.1.* Notice that for any  $W_1 \in \mathbb{R}^{n_d \times n_1}$

$$\begin{aligned} \mathbb{E}_{z_0, z_1} [\|W_1^*(W_0^* z_0 + z_1) - W_1 W_0^* z_0\|_2^2] &= \mathbb{E}_{z_0} [\|(W_1^* - W_1)W_0^* z_0\|_2^2] + \mathbb{E}_{z_1} [\|W_1^* z_1\|_2^2] \\ &= \|(W_1^* - W_1)W_0^*\|_F^2 + \|W_1^*\|_F^2, \end{aligned}$$

where the first equality used independence of  $z_0$  and  $z_1$  and the second used the fact that  $\mathbb{E}_{z \sim \mathcal{N}(0, I_n)} \|Mz\|_2^2 = \|M\|_F^2$  for any matrix  $M \in \mathbb{R}^{m \times n}$ . The solutions of (2) are then solutions of

$$\min_{W_1 \in \mathbb{R}^{n_1 \times n_0}} \|\mathcal{L}(W_1^*) - \mathcal{L}(W_1)\|_F^2 \quad (6)$$

where  $\mathcal{L} : \mathbb{R}^{n_d \times n_1} \rightarrow \mathbb{R}^{n_1 \times n_0}$  is the linear operator given by  $\mathcal{L} : W_1 \mapsto W_1 W_0^*$ . Since  $n_1 > n_0$ , this operator is singular and there are infinite solutions of (6), all of which satisfy  $\mathcal{L}(W_1^*) = \mathcal{L}(W_1)$ , i.e. the thesis.

Regarding (3), observe instead that for any  $W_1 \in \mathbb{R}^{n_d \times n_1}$

$$\mathbb{E}_{z_0, z_1} [\|W_1^*(W_0^* z_0 + z_1) - W_1(W_0^* z_0 + z_1)\|_2^2] = \|(W_1^* - W_1)W_0^*\|_F^2 + \|W_1^* - W_1\|_F^2.$$

This shows  $W_1 = W_1^*$  is the unique minimizer of (3).  $\square$

Before analyzing the solution of compressed sensing with the trained generative models, we observe the following fact on the minimum norm solution of (2).

**Lemma B.1.** *Let  $W_1^{\text{Van}}$  be the minimum Frobenius norm solution of (2). Then  $W_1^{\text{Van}} = W_1^* W_0^* (W_0^*)^\dagger$  where  $(W_0^*)^\dagger$  is the pseudoinverse of  $W_0^*$ .*

*Proof.* Notice that  $\mathcal{L}(W_1^*) = \mathcal{L}(W_1^{\text{Van}})$ , where  $\mathcal{L}$  is defined in the proof of Lemma (5.1). We next show that  $W_1^{\text{Van}}$  is orthogonal to the null space of  $\mathcal{L}$ , which implies the thesis.

Let  $W_1 \in \mathbb{R}^{n_d \times n_1}$  be such that  $\mathcal{L}(W_1) = W_1 W_0^* = 0$ . Then we have

$$\begin{aligned} \langle W_1^{\text{Van}}, W_1 \rangle_F &= \text{tr}((W_1^{\text{Van}})^T W_1) \\ &= \text{tr}(W_1 (W_0^* (W_0^*)^\dagger)^T (W_1^*)^T) \\ &= \text{tr}(W_1 W_0^* (W_0^*)^\dagger (W_1^*)^T) \\ &= 0, \end{aligned}$$

where third equality uses the fact that  $W_0^* (W_0^*)^\dagger$  is symmetric and the fourth one the assumption on  $W_1$ .  $\square$

*Proof of Lemma 5.2.*

- Proof of (4). Notice that by the previous lemma  $W_1^{\text{Van}} = W_1^* W_0^* (W_0^*)^\dagger = W_1^* \mathcal{P}_{W_0^*}$  where  $\mathcal{P}_{W_0^*}$  is the orthogonal projector onto the range of  $W_0^*$ . Moreover, with probability 1,  $(AW_1^* W_0^*)$  is full rank. It follows then, that  $(z_0^{\text{van}}, z_1^{\text{van}})$  is given by

$$\begin{aligned} z_0^{\text{van}} &= \arg \min_{z_0 \in \mathbb{R}^{n_0}} \|y - AW_1^* W_0^* z_0\|_2^2, \\ z_1^{\text{van}} &= \arg \min_{z_1 \in \mathbb{R}^{n_1}} \|y - AW_1^* (W_0^* z_0^{(0)} + \mathcal{P}_{W_0^*} z_1)\|_2^2. \end{aligned}$$

In particular the minimum norm solution  $z_1^{\text{van}}$  will satisfies  $(I - \mathcal{P}_{W_0^*})z_1^{\text{van}} = 0$ . We have therefore  $\tilde{G}^{\text{Van}}(z_0^{\text{van}}, z_1^{\text{van}}) = W_1^* (W_0^* z_0^* + W_0^* \mathcal{M}_1 z_1^*)$  where  $\mathcal{M}_1 = (AW_1^* W_0^*)^\dagger W_1^*$ .

The reconstruction error is then given by

$$\begin{aligned} \mathbb{E}_{z_0^*, z_1^*} \|G^*(z_0^*, z_1^*) - \tilde{G}^{\text{Van}}(z_0^{\text{van}}, z_1^{\text{van}})\|_2^2 &= \|W_1^* - W_1^* W_0^* \mathcal{M}_1\|_F^2 \\ &\geq \min_{\mathcal{M} \in \mathbb{R}^{n_0 \times n_1}} \|W_1^* - W_1^* W_0^* \mathcal{M}\|_F^2 \\ &= \|(I_{n_d} - \mathcal{P}_{W_1^* W_0^*})W_1^*\|_F^2 \end{aligned}$$

where the first equality follows from the properties of the normal distribution. Regarding then the minimization problem  $\min_{\mathcal{M} \in \mathbb{R}^{n_0 \times n_1}} \|W_1^* - W_1^* W_0^* \mathcal{M}_1\|_F^2$ , notice that this is convex and the critical points satisfy

$$(W_1^* W_0^*)^T W_1^* = (W_1^* W_0^*)^T (W_1^* W_0^*) \mathcal{M}$$

Using the fact that  $W_1^* W_0^*$  is full rank, the unique solution is found to be  $[(W_1^* W_0^*)^T (W_1^* W_0^*)]^{-1} (W_1^* W_0^*)^T W_1^*$ , which gives the last equality.

Note now that  $\mathcal{P}_{W_1^* W_0^*}$  is the projector onto the range of  $W_1^* W_0^*$  and  $W_1^*$  is full rank. Thus

$$\|(I_{n_d} - \mathcal{P}_{W_1^* W_0^*}) W_1^*\|_F^2 \geq \|(I_{n_d} - \mathcal{P}_{W_1^* W_0^*}) W_1^*\|_2^2 = \max_{h \in \text{range}(W_0^*)^\perp} \|(I_{n_d} - \mathcal{P}_{W_1^* W_0^*}) W_1^* h\|_2^2 > 0.$$

- *Proof of (5)* Notice again that with probability 1,  $AW_1^* W_0^*$  and  $AW_1^*$  have full rank. Moreover  $\tilde{G}^{\text{RTIL}}(z_0^{\text{rtil}}, z_1^{\text{rtil}}) = W_1^* (W_0^* z_0^{\text{rtil}} + z_1^{\text{rtil}})$  where

$$\begin{aligned} z_0^{\text{rtil}} &= \arg \min_{z_0 \in \mathbb{R}^{n_0}} \|y - AW_1^{\text{RTIL}} W_0^* z_0\|_2^2, \\ z_1^{\text{rtil}} &= \arg \min_{z_1 \in \mathbb{R}^{n_1}} \|y - AW_1^{\text{RTIL}} (W_0^* z_0^{\text{rtil}} + z_1)\|_2^2. \end{aligned}$$

It is then easy to see that

$$\begin{aligned} z_0^{\text{rtil}} &= z_0^* + (AW_1^* W_0^*)^\dagger AW_1^* z_1^* \\ z_1^{\text{rtil}} &= z_1^* - W_0^* (AW_1^* W_0^*)^\dagger AW_1^* z_1^* \end{aligned}$$

where  $(AW_1^* W_0^*)^\dagger$  denotes the pseudoinverse of  $(AW_1^* W_0^*)$ . It then follows that  $W_1^* (W_0^* z_0^{\text{rtil}} + z_1^{\text{rtil}}) = W_1^* (W_0^* z_0^* + z_1^*) = x^*$ , which implies the thesis.  $\square$